Resolution Dependency of the Diurnal Cycle of Convective Clouds over the Tibetan Plateau in a Mesoscale Model

Tomonori SATO

Center for Climate System Research, University of Tokyo, Kashiwa, Japan

Takao YOSHIKANE

Frontier Research Center for Global Change, Japan Agency for Marine-Earth Science and Technology, Yokohama, Japan

Masaki SATOH

Center for Climate System Research, University of Tokyo, Kashiwa, Japan
Frontier Research Center for Global Change, Japan Agency for Marine-Earth Science and Technology, Yokohama, Japan

Hiroaki MIURA

Frontier Research Center for Global Change, Japan Agency for Marine-Earth Science and Technology, Yokohama, Japan

and

Hatsuki FUJINAMI

Hydrospheric Atmospheric Research Center, Nagoya University, Nagoya, Japan

(*Manuscript received 31 July 2007, in final form 29 February 2008*)

Abstract

Sensitivity of precipitation diurnal cycle to the horizontal grid spacing was investigated using a mesoscale model without cumulus parameterization. Four numerical experiments with changing horizontal resolution are performed over one month with NCEP reanalysis boundary forcing. The studied range of grid spacing is from 3.5 km to 28 km which has been known as the intermediate scale to simulate mesoscale systems with/without cumulus parameterization. The target area is the Tibetan Plateau where pronounced diurnal cycle of convective systems is observed during the spring season.

Lower resolution runs (14 and 28 km grid) show delayed formation and delayed mature stage of the cumulus convection in comparison to satellite observations. On the other hand, higher resolution runs (3.5 and 7 km grid) reproduce the proper development of the clouds after local noon which is consistent with observations. The total hydrometeor content and rainfall rate increase with grid size. Such systematic relationship of resolution dependencies are confirmed even in the monthly mean diurnal cycle, although most of previous studies examined only short periods. These results suggest that finer resolution at less than 7 kilometer is necessary to simulate realistic phase of the precipitation diurnal cycle over the Tibetan Plateau.

The mechanism that is responsible for the resolution dependency is discussed. We suggest that the

daytime convection which initially occurs due to unstable stratification over the Tibetan Plateau in spring tends to have a horizontal scale smaller than that is resolvable by the coarse resolution runs. The delayed cloud formation induces larger downward shortwave radiation, which increases surface fluxes and results in too strong rainfall in the coarser resolution runs.

1. Introduction

The diurnal cycle of precipitation is a pronounced feature (e.g., Dai 2001) that has a large contribution to the total precipitation variability over the low and middle latitude regions. Latent heating released in the precipitation system is one important energy source that drives the circulation in the troposphere. Thus, the diurnal cycle of precipitation is also an inevitable aspect of the climate system (Neale and Slingo 2003; Dai and Trenberth 2004). The conventional General Circulation Models (GCMs), which have horizontal resolution in the order of 100 kilometers, use cumulus parameterizations (such as Arakawa and Schubert 1974; Kuo 1974) to deal with the cumulus convection whose horizontal scale is smaller than the grid size. Recently, many studies have pointed out difficulties to simulate the phase of the precipitation diurnal cycle in the GCMs with cumulus parameterization (Dai 2006; Collier and Bowman 2004). Dai (2006) showed that the phase of the diurnal cycle over land is still different (too early) from the observed one in the latest generation of GCMs.

In order to reduce the uncertainties resulting from cumulus parameterization, sophisticated treatment of convection in GCMs have been developed by some groups. Grabowski (2001) and Khairoutdinov and Randall (2001) proposed the MMF (Multi-scale Modeling Framework) in which a Cloud-Resolving Model (CRM) is used to replace the parameterization in a coarse resolution GCM. The Nonhydrostatic ICosahedral Atmospheric Model (NICAM) has been developed by Frontier Research Center for Global Change (FRCGC) and Center for Climate System Research (CCSR), University of Tokyo (Tomita and Satoh 2004; Satoh et al. 2007). With a few kilometers mesh interval over the globe, NICAM is intended to resolve mesoscale circulations associated with deep convection by calculating explicit cloud physics instead of cumulus parameterizations. The NICAM performed one month simulation at 3.5 km mesh grid without cumulus parameterization (Tomita et al. 2005; Miura et al. 2005). So far, simulations of typhoon development (Miura et al. 2007a) and propagation of the Madden-Julian oscillation (Miura et al. 2007b) were succeeded in the NICAM with realistic land-ocean distribution. Although numerical experiments using NICAM are carried out mainly by the Earth Simulator, high resolution experiments, like 3.5 km mesh run, are still hard in respect of the computational cost. Therefore, coarser resolution runs are simultaneously carried out for test runs related to the model development.

Molinari and Dudek (1992) summarized the ideal grid size in case with/without cumulus parameterization in numerical models. Since the cumulus parameterization generally considers a group of cumulus convections in a grid box, grid spacing larger than approximately 20–30 km is desired when one uses the cumulus parameterization in GCMs. On the other hand, cloud-resolving or cloud-system-resolving model should be run with grid size smaller than a few kilometers in order to secure enough grid points within a cloud system. Therefore, our knowledge on the behaviors of numerical models whose horizontal grid size is between a few kilometers and 20 km are very much limited.

Generally, the mesoscale models, which cover a certain area of interest by giving a boundary forcing data, are easy to apply for cloud resolving simulations because of its lower computational cost. Many studies have already focused on the sensitivity of the simulated results to horizontal grid spacing. The previous studies investigated in a broad spectral range of the horizontal grid size from the order of 1 m up to the order of 10 km (e.g., Stevens et al. 2002; Weisman et al. 1997; Bryan et al. 2003; Murata et al. 2003; Nagasawa et al. 2006). Some of the studies show that the characteristics (such as maximum intensity and life time) of the simulated mesoscale convective systems vary with the horizontal grid size even without a cumulus parameterization in the mesoscale model (Weisman et al. 1997; Petch et al. 2002). Weisman et al.

Corresponding author: Tomonori Sato, Center for Climate System Research, University of Tokyo, 5-1-5 Kashiwanoha, Kashiwa, 277-8568, Japan
E-mail: t_sato@ccsr.u-tokyo.ac.jp

(1997) showed that the lifetime of the convective storm tends to be long and the intensity becomes stronger as grid size of the mesoscale model increases. However, the integration period in these experiments were generally very short, such as several days or even a few hours, because they were interested in mesoscale phenomena. Furthermore, since they were motivated to examine the dynamical frame and physical schemes in the model, sensitivity of grid size was investigated under somewhat unrealistic conditions, such as those done by two-dimensional models or those describing the convective systems which are initialized by the artificial warm bubble in the model. Petch et al. (2002) examined the sensitivity to horizontal resolution in a viewpoint of precipitation diurnal cycle, and found that the diurnal maximum occurs earlier as the horizontal resolution becomes higher. However, they also carried out only for a few days of integration by a two-dimensional model. Thus, there is a need to study the resolution dependency of the precipitation diurnal cycle under more realistic atmospheric conditions. Sato et al. (2007) showed using NICAM experiments that the diurnal cycle of convective activities over the Tibetan Plateau tends to be closer to observations as the grid interval becomes smaller. Unfortunately, the period of the analysis was only seven days due to huge computational cost, which may be not enough to describe the resolution dependency under the realistic conditions owing to the large variability in atmospheric processes.

In this study, we investigate the detailed feature of resolution dependency from the four one-month experiments changing the grid interval in a mesoscale model. The studied range of horizontal grid size is from 3.5 km to 28 km which has been known as the intermediate scale to either use or not use a cumulus parameterization. Implications of this study will be useful to evaluate the diurnal cycle of precipitation simulated in the CRMs which have the horizontal resolution of this range.

2. Model simulations and observational data

2.1 Model simulations

The simulated region is the Tibetan Plateau which was already studied by Sato et al. (2007) using the NICAM data. The Tibetan Plateau was selected because of its large influences on the continental to global-scale climate (e.g., Hahn and Manabe 1975; Wu and Zhang 1998; Sato and Kimura 2005, 2007; Liu et al. 2007). The studied period is April of 2004 over which Miura et al. (2007a) performed the realistic global simulation. Over the Tibetan Plateau the diurnal cycle of convective systems becomes pronounced in April (Fujinami and Yasunari 2001).

The Weather Research and Forecasting (WRF) model (Skamarock et al. 2005), which was developed by the collaboration study among the National Center for Atmospheric Research (NCAR), the National Oceanic and Atmospheric Administration the National Centers for Environmental Prediction (NCEP), the Forecast Systems Laboratory (FSL), the Air Force Weather Agency (AFWA), the Naval Research Laboratory, Oklahoma University, and the Federal Aviation Administration (FAA). The detail configuration of the model is shown in Table 1. The WRF Single-Moment 6-class (WSM6) scheme, which is one of the available microphysics schemes, was used as the precipitation formation process in the experiments. A summary of the experimental setup is given in Table 2. In all experiments, the NCEP final analysis data on one-degree grid every 6 hours was used as the initial and the

Table 1. Outline of the model.

Weather Research and Forecasting (WRF) modeling system Ver. 2.2

Dynamical Features	
Compressible, nonhydrostatic Euler equations.	
Terrain-following hydrostatic-pressure vertical coordinate	
Physical Features	
Microphysics	WRF Single-Moment 6-class (WSM6)
Boundary layer parameterization	Mellor-Yamada-Janjic TKE scheme (Janjic 2002)
Land-surface model	Noah land-surface model (Chen and Dudhia 2001)
Longwave radiation	Rapid Radiative Transfer Model (RRTM) (Mlawer et al. 1997)
Shortwave radiation	Dudhia scheme (Dudhia 1989)

Table 2. Experimental setup of the model. Numerical domains are shown in Fig. 1.

Calculation condition	
Surface and lateral boundary	NCEP final analysis (one degree grid, every 6 hours)
Vegetation	USGS 30 sec dataset in 1992
Simulation term	Started at 0 UTC 1 April, ended at 18 UTC 30 April 2004
Map projection	Lambert conformal
Center point of domain	90°E, 33°N
Number of Vertical layer	31

lateral boundary atmospheric conditions and the initial soil condition. The simulation started at 0 UTC 1 April 2004 and ended at 18 UTC 30 April 2004.

The numerical experiments are listed in Table 3. We conducted four experiments with the grid spacing of 3.5 km, 7 km, 14 km, and 28 km (hereinafter G3.5, G7, G14, and G28 runs, respectively), from which 3-hourly outputs were analyzed. The G3.5 and G7 runs applied the nesting technique in the 14 km-mesh and 28 km-mesh of the coarse mesh domains, respectively. The G14 and G28 runs are conducted without nesting domain. All numerical experiments were carried out without cumulus parameterization. Figure 1 shows the calculation domains and topography over the studied area. Figure 2 shows the cross sections of the topography along 87.5°E, which indicates that topographic complexities are quite different among the sensitivity experiments.

In order to evaluate the model results quantitatively and to compare them to the satellite observations, a radiative transfer model, which was developed at Japan Meteorological Agency, was used (Owada 2006). The radiative transfer model estimates the brightness temperature corresponding to the sensors boarded on the Geostationary Meteorological Satellite (GMS) using the three-dimensional structures of microphysical parameters and meteorological elements in the model.

2.2 Satellite data

Hourly observations provided by the geostationary satellite are quite useful to evaluate the diurnal cycle of convective activities in the model (e.g., Slingo et al. 2004; Sato et al. 2007). In this study, we used the statistics from infrared channel of GMS5, resolution of which is about 17 km over central Tibetan Plateau, to compare with one-month mean characteristics of the model results in Section 3.2. However, since the GMS5 was not in operation in April 2004, we also used the Geostationary Operational Environmental Satellite (GOES) 9 data to show one typical event of the diurnal cycle in Section 3.1. Since the resolution of GOES9 is approximately 50 km over central Tibetan Plateau, we just briefly describe the diurnal cycle of cloud activity.

3. Result

3.1 The diurnal cycle in 4 April 2004

Firstly, we compare the diurnal cycle of cloud activity between that observed by GOES9 and that simulated by the four sensitivity experiments. The target day is the 4th April in 2004 when pronounced developments of the convective systems were observed in the daytime. The environmental condition was very similar to the typical pattern representing the active phase of the diurnal cycle of convection which was shown in Fujinami and Yasunari (2001). The subtropical jet in the upper troposphere was splitting to the north and south of the Tibetan Plateau, and wind velocity over the Tibetan Plateau became very weak. Relatively cold air with 230 K extended over the plateau in the 300

Table 3. List of sensitivity experiments. Sizes of the numerical domains are shown in Fig. 1. Results from shaded parts were used for analysis.

	G28	G14	G7	G3.5
Nesting	Off	Off	On	On
Coarse mesh grid spacing (grid number)	28 km (120 × 90)	14 km (240 × 180)	28 km (120 × 90)	14 km (240 × 180)
Fine mesh grid spacing (grid number)			7 km (401 × 273)	3.5 km (797 × 541)

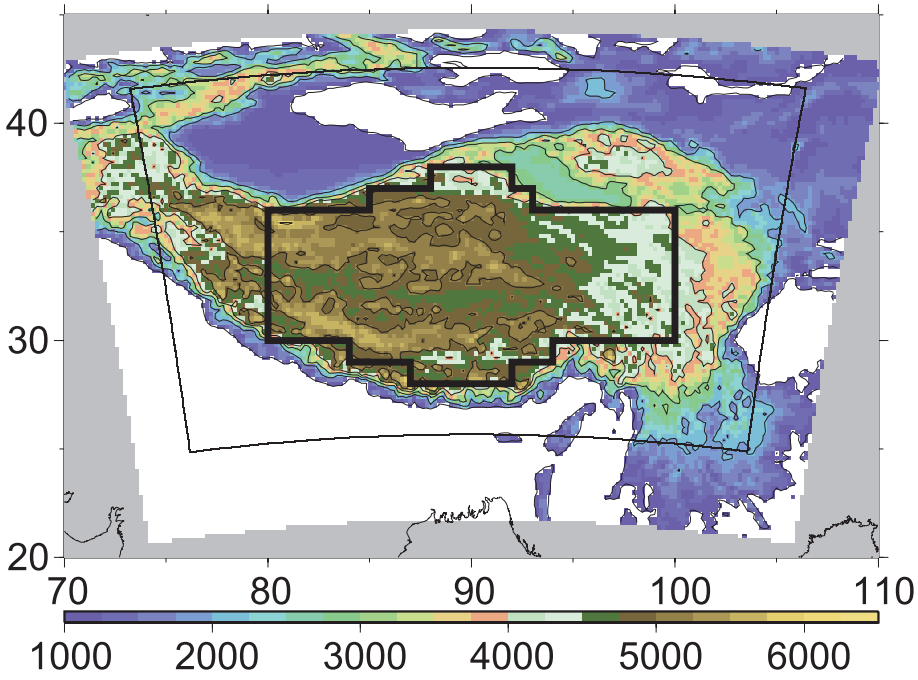

Fig. 1. Topography (m) in the numerical domain. Thin solid line indicates the area of the nested domain for G7 and G3.5 runs. Thick solid line indicates the area of the Tibetan Plateau used in Figs. 6, 7, and 8.

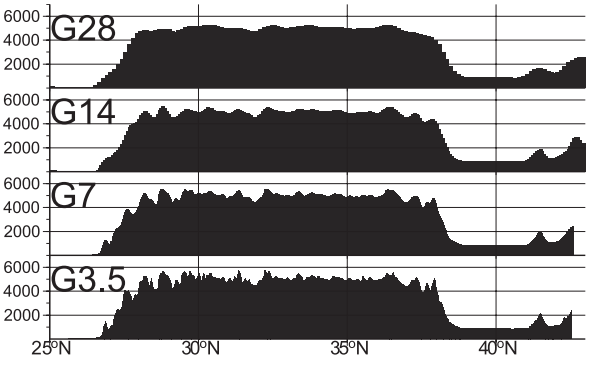

Fig. 2. Cross sections of the model topography (m) along 87.5°E.

hPa level (not shown). Those conditions seem to be favorable for convective systems to develop as the surface temperature rises during the daytime.

The diurnal variation of brightness temperature observed by GOES9 is shown in Fig. 3. Clouds sparsely existed in the morning except for some high level clouds. At 12 LT (Local Time; LT = UTC + 6), many small clouds are formed in the central and western Tibetan Plateau. At the same time brightness temperature of the larger cloud systems over the eastern plateau decreases, indicating the development of high clouds. Cloud systems were developing at 15 LT, and high clouds completely cover the whole area of the plateau by 18 LT. After the sunset some high clouds remain, but, their cloud top heights were decreasing by 22 LT. As a result, nearly half of the region can be recognized as cloud free areas. At 24 LT, clouds were further decayed and higher brightness temperatures, which denote the land surface, can be seen from the satellite over large areas of the plateau.

Figure 4 depicts the diurnal cycle of vertically integrated hydrometeors in the four WRF experiments for 4 April 2004. Values in G3.5, G7, and G14 are horizontally averaged at G28 grid points. In each run, the model simulates clouds over eastern plateau in the morning (noted as A in Fig. 4). The difference among the runs is pronounced at 12 LT. In G3.5 and G7 runs, numerous small-scale clouds appear over the central and western plateau (noted as B in Fig. 4) whereas there are few such clouds in the G14 and G28 runs. Cloud formation in the G14 run is more concentrated in the southwestern part of the plateau. In the G28 run, clouds

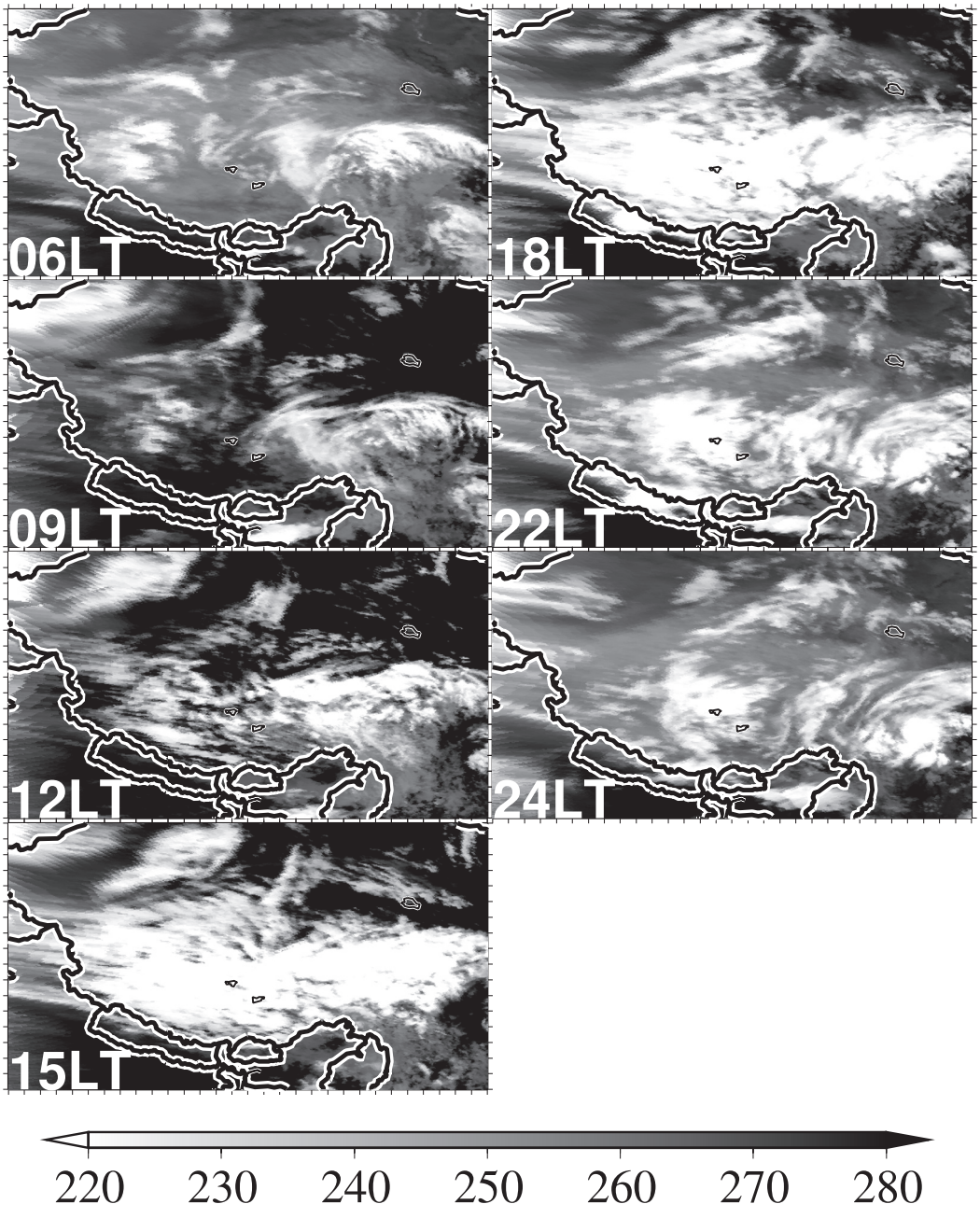

Fig. 3. Brightness temperature (K) around the Tibetan Plateau in 4 April 2004 observed by GOES9. Each panel covers 75–105°E, 25–42°N. (a) 06 LT, (b) 09 LT, (c) 12 LT, (d) 15 LT, (e) 18 LT, (f) 22 LT, and (g) 24 LT. Data was not available for 21 LT.

over western plateau are absent, although they are actually observed by the satellite and simulated in the G3.5 and G7 runs. On the other hand, the development of the observed clouds over the eastern plateau (cloud system A) is evident in all the experiments. The cloud system A indicates the development at 12 LT as well as the cloud system B. The generations of the clouds in region B are found in both G14 and G28 runs at 15 LT. It is notable that the hydrometeor content becomes larger as the grid size increases. At 18 LT clouds in region B begin to decay, and the number of clouds

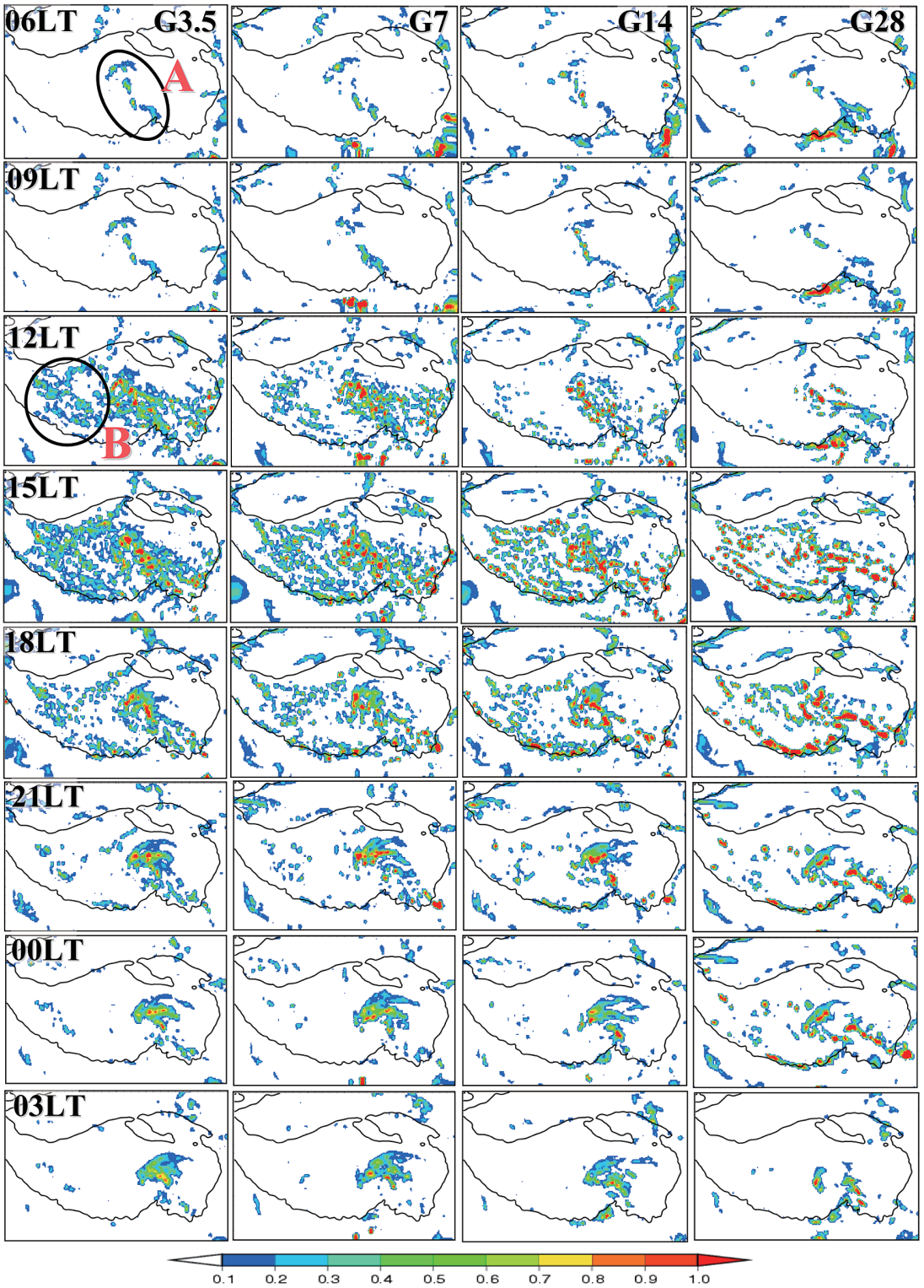

Fig. 4. Diurnal change of vertically integrated condensed water (kg m^{-2}) around the Tibetan Plateau in 4 April 2004 simulated by four sensitivity experiments. Figures are drawn over 75–105°E 25–42°N. Solid lines indicate the 3000 m topography. Values in G3.5, G7, and G14 are horizontally averaged at G28 grid points.

decreases. Most of the small clouds decease until 21 LT in central and western plateau, which agrees with the satellite observations. At midnight, the small clouds completely disappear over the Tibetan Plateau. The WRF simulations capture well the diurnal cycle of the cloud patterns for this particular day, which seems to be representative of the typical diurnal cycle over this region.

A latitude-height cross section of the mixing ratio of the condensed water is shown in Fig. 5, in which the variables in G3.5, G7, and G14 are averaged for drawing the figures with the same grid point with G28. Marked difference in the vertical structure also appears at 12 LT. The deep convection existing to the whole troposphere is seen in the G3.5 run. The height of the convection in the G7 run is similar to that in the G3.5 run, but the number of the convection towers is smaller. On the other hand, the number of convective clouds is very small in both G14 and G28 runs. At 15 LT, many cloud systems are still present in the G3.5 run. The number of deep convective clouds is greatly increased in G7, G14, and G28 runs compared with those at 12 LT. The horizontal scale of each convective system is larger in G28 run, characterized by the distributed cores, than those in the G3.5 and G7 runs.

These results clearly indicate that the formation time of the cumulus clouds is quite different even in the realistic simulation over complex terrain owing to the choice of the grid size in the model. Cloud formations in the G14 and G28 runs are about three-hour later than those in the G3.5 and G7 runs. Monthly mean characteristics of the cloud and precipitation diurnal cycle are described in the next section followed by discussions on the simulated differences in the cloud features in Section 4.

3.2 Monthly average view

Diurnal variations of clouds over western and central plateau shown in Section 3.1 are very similar to those in the monthly mean cloud characteristics in terms of the cloud distribution. Thus, here we mainly focus on the cloud statistics, especially the diurnal cycle of area-averaged monthly-mean clouds and precipitation properties for April 2004.

Figure 6 shows the monthly mean diurnal variation of hydrometeor content over the Tibetan Plateau (see Fig. 1) simulated by the model. In G3.5 and G7 runs, total hydrometeor rapidly increases after 9 LT while the increases come later in G14 and G28 runs. The daily maximum hydrometeor contents occur at 15 LT in all runs. The amount decreases after 15 LT in all runs, with G28 decreasing at a slower pace. Consequently, cloud mixing ratio remains largest after sunset in the G28 run.

Diurnal variations of monthly mean precipitation

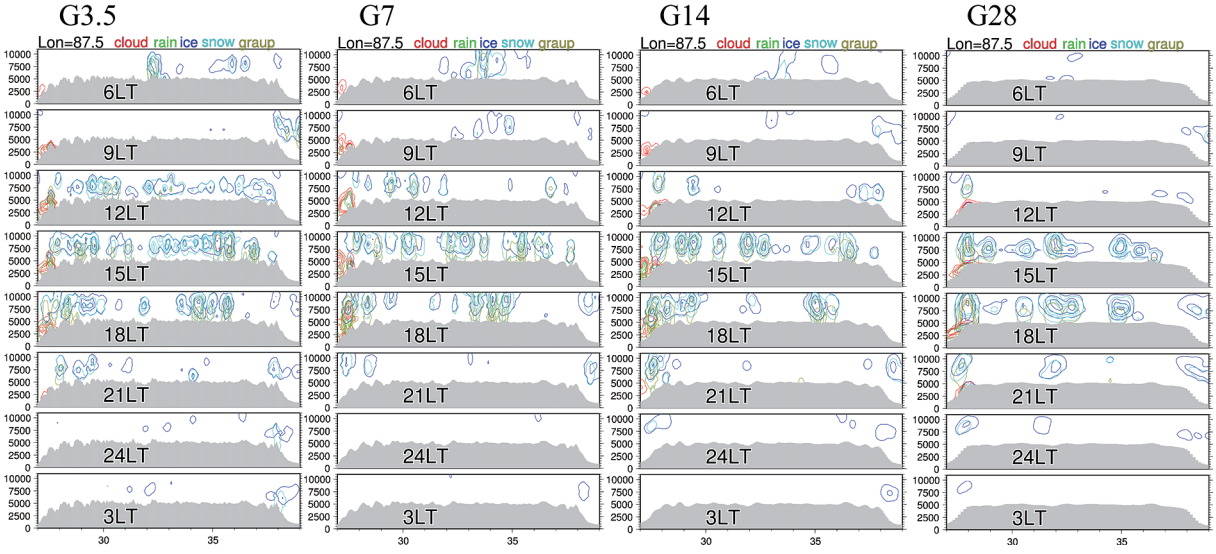

Fig. 5. Diurnal change of the vertical cross section of cloud mixing ratio along 87.5°E in 4 April 2004 simulated by four sensitivity experiments. Contour intervals are 5×10^{-3} [kg/kg]. Values are horizontally averaged in G3.5, G7, and G14 for drawing the figures with the same grid interval with G28.

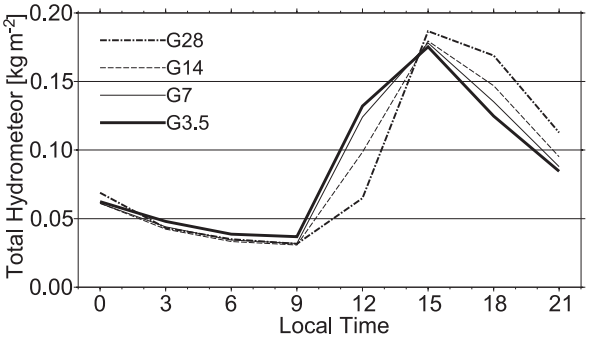

Fig. 6. Monthly-mean diurnal variations of vertically-integrated total hydrometeor content over the Tibetan Plateau (see Fig. 1).

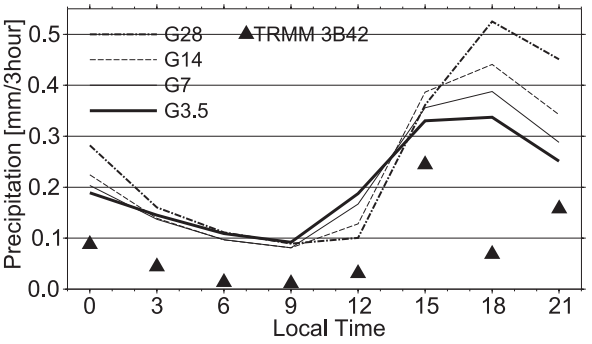

Fig. 7. Same as Fig. 6 but for precipitation. Observed estimations in April 2004 based on TRMM 3B42 product are also drawn as triangles.

(Fig. 7) show very similar characteristics to the hydrometeor content. The area-mean precipitation is lower in G28 and G14 runs than in G3.5 and G7 runs at 12 LT. In G3.5 and G7 runs, precipitation starts during 9–12 LT. To the contrary, this relationship is opposite at 18 LT, in which the rainfall amount is largest in G28 run and smallest in G3.5 run, suggesting that the nighttime precipitation is also sensitive to the grid size. The diurnal maximum occurs around 18 LT in G28, G14, and G7 runs while precipitation rates at 15 LT and 18 LT are almost the same in G3.5 run. The daily total precipitation is largest in G28 run, and decreases with smaller grid-size, indicating very systematic relationship to the model resolution. In comparison to the satellite estimation based on the TRMM 3B42 product, the model tends to overestimate the rainfall over the Tibetan Plateau, although the 3B42 product also contains uncertainties when it uses the infrared channel observation to estimate rainfall. The TRMM 3B42 data was also reported to show later maximum than that of the surface observation (Dai et al. 2007). The rainfall intensity in 3B42 dataset seems to be stronger in comparison to the seasonal mean values based on TRMM PR observation (Hirose and Nakamura 2005) although the analyzed area slightly differs from that in the current study. The simulated diurnal cycle is in good agreement to the observed one.

Figure 8 shows the diurnal variations of probability density (PD) of brightness temperature for satellite observations and the WRF simulations. The statistical analysis was performed only for the Tibetan Plateau as shown in Fig. 1. Brightness temperatures in the WRF simulations were computed using a radiation transfer model (see Section 2.1). The daily mean PD from five-year statistics of the GMS observations shows sharp maximum at 265 K indicating the surface temperature of the plateau (Fig. 8a). The PD at 18 LT has two peaks around 230 K and 270 K. Similar pattern of diurnal cycle are reproduced in all sensitivity runs. At 18 LT, the PD tends to show lower value around 230 K and higher value around 270 K in comparison to the GMS observation (Figs. 8b, c). These results indicate that in the afternoon the cloud cover is too small even in G3.5 run. Diurnal changes of PD show good resembling to the observations. After 18 LT, the signals indicating high-level clouds are decreased, and very high density appears around 265–270 K throughout the night corresponding to the surface temperature in the cloud free areas. The G3.5 run well captures the observed cloud formation in the afternoon, although the PD (i.e., cloud frequency and cloud cover) is still low. Disappearance of the high clouds is also in good agreement with the observation. On the other hand, the formation time of the clouds is too late in G28 run, resulting in a diurnal peak of PD around 230 K at 18 LT. Additionally, the disappearance of the high clouds is also delayed in the G28 run, which results in absorbing the longwave radiation from the ground surface during the night.

4. Discussions

4.1 Factors responsible for the resolution dependency

We investigated the sensitivity of the precipitation diurnal cycle over the complex terrain by changing model resolution. The results indicate that the phase and the amplitude of diurnal cycle

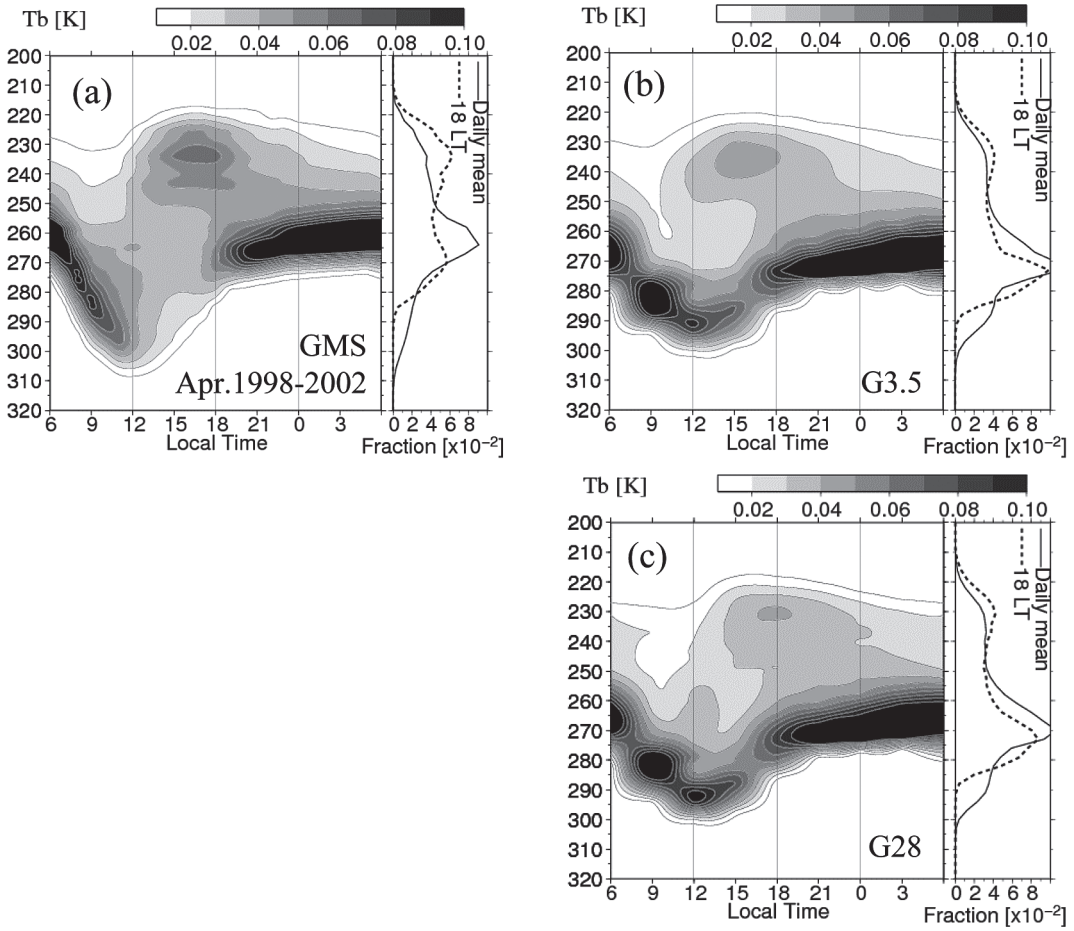

Fig. 8. Diurnal variations of the probability density of brightness temperature over the Tibetan Plateau (see Fig. 1). (a) GMS5 observation in April during 1998–2002. (b) G3.5. (c) G28.

are strongly dependent on grid size of the model. In this subsection, the resolution dependencies revealed in Section 3 are discussed in association with the controlling physical processes.

Representation of the model topography (cf., Fig. 2) may be a significant factor which causes the different behaviors of convective systems because in summer monsoon season mountain-valley circulation plays an important role controlling diurnal cycle of rainfall and clouds (Kuwagawa et al. 2001; Kurosaki and Kimura 2002). Figure 9 shows the diurnal variations of low-level wind convergence along 87.5°E. The magnitude of the convergence in each experiment clearly shows close relationship to the model resolution indicating stronger convergence/divergence as grid interval decreases. In G3.5 and G7 daytime convergences over the Himalaya around 27.5°N and southern plateau around 30°N is evident while they are very weak in G14 and absent in G28. Over the plateau (30–37°N) daytime-nighttime alternation of the convergence and divergence is very dominant in G3.5 corresponding to the topography whereas it is very weak in G28. From these aspects, topographic contrast in the plateau seems to be an important factor to form the convergence pattern in lower atmosphere. However, as we showed in Fig. 4 and Fig. 5, diurnal change of clouds is evident in G28 in spite of the smooth topography and the weak low-level convergence. Thus, the topographic effect is not always a necessary factor to initiate clouds or to cause phase difference of the diurnal cycle.

The daytime convection cells over the Tibetan Plateau consist of tall cumulus-type clouds whose top reaches at tropopause as seen in Fig. 5. The lifetime of each cloud system is not very long since

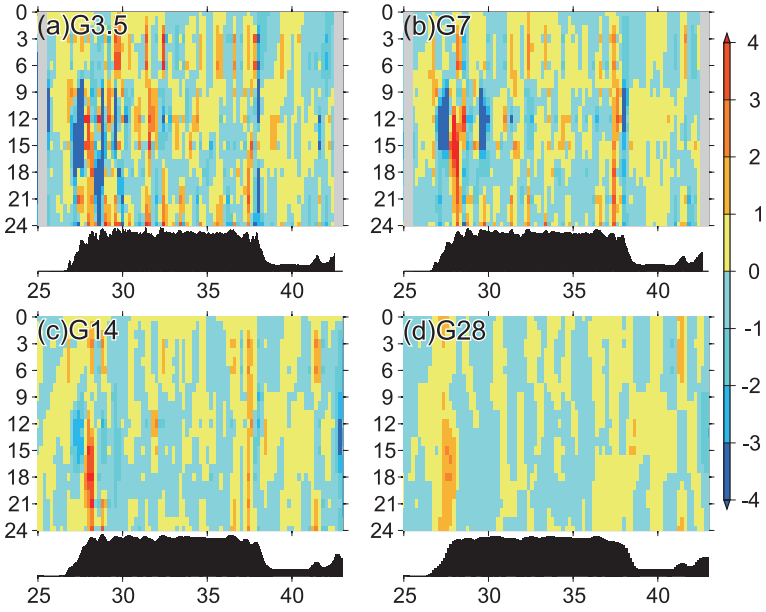

Fig. 9. Monthly-mean diurnal variations of convergence (10^{-5} sec^{-1}) at 10 m level along 87.5°E in (a) G3.5, (b) G7, (c) G14, and (d) G28 runs. Positive values indicate divergence. Values in G3.5, G7, and G14 are averaged to have the same grid spacing with G28. Topographies along the cross section are shown below.

it generates around noon and disappears after sunset. Fujinami and Yasunari (2001) indicated that the formation of spring season convection occurs as a result of unstable stratification due to both the upper cold air and the daytime surface heating when environmental wind is not strong. According to the Bènard-Rayleigh convection theory, critical horizontal wavelength of the convection (k_c) can be expressed as $k_c = \pi/\sqrt{2} \approx 2.22$. Over the Tibetan Plateau if we simply assume the depth of convection (H) be 5-6 km, the convection which is firstly initiated by the vertical potential temperature gradient will have the horizontal scale of $H \times k_c \approx 11$ –13 km. Therefore, G14, G28, and G7 do not have sufficient resolution to simulate the convection that initially occurs after the Rayleigh number exceeds its critical value (R_c). As the unstable stratification becomes stronger, vertical convection which has larger horizontal scale can be developed. Therefore, relatively lower resolution runs are capable of resolving the convection at this moment, although its intensity may be too strong due to the increased instability. The resultant convection causes stronger precipitation with its phase delayed in the coarser resolution run. One has to note that the theoretical approach should be limited to the qualitative comparison because of its assumptions for simplicity, thus, we cannot directly apply it to the realistic cases of convective initialization. Additionally, we cannot quantitatively compare the critical Rayleigh numbers derived from the theory and the numerical experiments. The theoretical evaluation is very useful as long as to show the qualitative relationship of the resolvable convection sizes in each experiment against the realistic convection sizes. It is very clear that a finer resolution run leads to early maximum of convection while a coarser resolution run leads to the late maximum with strong intensity. In the past study effective upward moisture transport was suggested to be important for initiation of the deep convection (Petch et al. 2002; Shinoda and Uyeda 2002). In the current study, efficiency of the vertical moisture transport by the grid-scale and subgrid-scale vertical motion is one of the important processes which may cause the phase difference. In the spring season over the Tibetan Plateau, however, the atmosphere contains very little moisture, and the unstable stratification of the atmosphere becomes dominant while convective instability becomes significant in monsoon season (Fujinami and Yasunari 2001).

In G3.5 cloud formation clearly takes place along

the mountain range (Fig. 5). Over the mountain area the height of vertical convection is lower due to the elevated surface than that potentially occurs over the valley. Thus, the Rayleigh number exceeds its critical value (R_c) with relatively weaker surface heating. Therefore, the convective clouds are likely to occur over the mountain than those over the valley. Clouds generate frequently over the mountain even without the horizontal moisture transport by the mountain-valley circulation, which is totally different from that known in the summer season (Kuwagata et al. 2001).

The delayed cloud formation conducts to the difference of surface energy budget in coarse resolution runs. Around local noon surface heat flux in G28 becomes larger than other experiments because, owing to the delayed cloud formation, the downward shortwave radiation is higher without any interception by the clouds. Therefore, if daytime convection occurs in G28, it is more intense than other runs according to the larger sensible heat flux.

The heavier rainfall in G28 induces high soil moisture content. Relatively larger evaporation in G28 tends to produce further delay of convection start in the next day. This is the positive feedback by the land surface processes indicating that a coarse resolution causes strong intensity and delayed diurnal cycle of rainfall. In other word, coarse resolution experiments tend to overestimate the water cycle, which implies the necessity to adopt proper grid size to study the water cycle. Our results indicate that the different grid size causes the differences of land-atmosphere interaction which also complicatedly responses to the diurnal cycle through the feedback mechanisms. In our experiments, initial conditions of soil moisture are the same among the experiments. Therefore, the differences in intensity and phase originally occur due to the limitation of resolvable convection size followed by the feedback mechanisms which further enhances the differences.

The results from sensitivity experiments indicate that the diurnal cycle of convective activity is quite sensitive to horizontal resolution of the model in spite of the longer-term integration. The resolution dependencies are enough to modulate clouds statistics including diurnal phase, amplitude, and frequencies, which likely to modulate the radiative balance and the hydrological cycles.

4.2 Implications to the global CRMs

As we have mentioned, horizontal grid size should be properly determined to simulate precipitation by cumulus and microphysics parameterizations. Since the cumulus parameterization usually assumes a group of cumulus in a model grid box, the grid size is desired to be larger than 20–30 km. On the other hand, in order to simulate precipitation systems without cumulus parameterization, the grid size should be at least smaller than a few kilometers. Our study ranges the grid size among them (3.5–28 km) which also covers the theory-based estimation of the horizontal scale of the Bènard convection.

Conventional GCMs using cumulus parameterization exhibit too early and heavy precipitation over land (Dai 2006). Arakawa and Kitoh (2005) suggested that the phase of the precipitation diurnal cycle becomes later (closer to observations) by the improved representation of topography in a 20 km-mesh GCM than that in a low-resolution

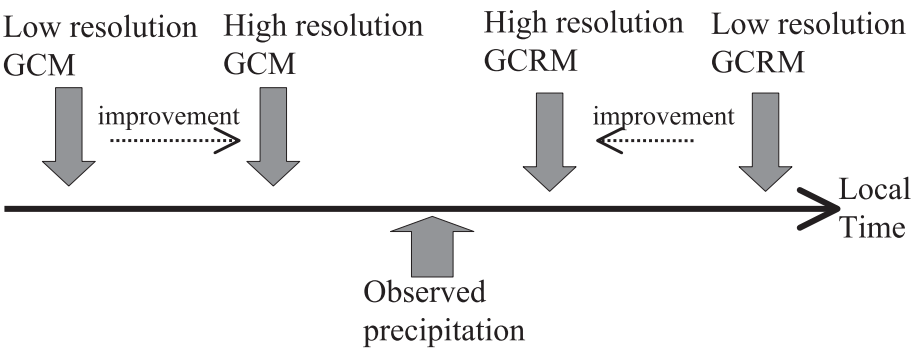

Fig. 10. Illustration showing the phase of precipitation diurnal cycle over land from different models and observation.

GCM (cf., Fig. 10). However, use of the cumulus parameterization in GCMs with grid interval less than 20–30 km may be out of target according to its physical concept behind. Thus, new generation general circulation model like NICAM is necessary in the future covering the globe without cumulus parameterization. As we have indicated, a Global Cloud Resolving Model (GCRM) is ought to do longer-term (one month or longer) simulation with a low-resolution mode which does not have enough resolution to explicitly resolve clouds. From the perspectives of previous studies and the current study, a low resolution GCRM would exhibit a later maximum of the diurnal cycle compared to that observed (Fig. 10). However, the diurnal cycle in GCRM is expected to be closer to the observation as we increase the horizontal resolution supported by increasing computer power, even though some discrepancies are currently recognized in low-resolution GCRM (Inoue et al. 2008).

Controlling physical processes and propagating mechanisms of the diurnal cycle of convective systems differ from region to region and/or season to season. Here we have shown one example of the diurnal cycle mainly excited by strongly unstable stratification. Further studies are necessary to investigate the relationship between model resolution and the simulated diurnal cycle under different environmental conditions such as in monsoon season or over tropical regions where the diurnal cycle of convection is more strongly affected by the behavior of atmospheric moisture.

5. Conclusion

In this study, we have investigated the sensitivity of the diurnal cycle of clouds and precipitation to the horizontal grid size of a mesoscale model. Four numerical experiments with changing horizontal resolution were performed for April 2004 with NCEP reanalysis boundary forcing. The grid size ranges from 3.5 km to 28 km which has been known as the intermediate scale for simulating mesoscale systems with/without cumulus parameterization. All numerical experiments were conducted without cumulus parameterization. The target area is the Tibetan Plateau where pronounced diurnal cycles of convective systems are observed during the spring season.

Lower resolution runs (14–28 km grid) tend to show delayed formations and delayed mature stages of the cumulus convection in comparison to the satellite observations. On the other hand, higher resolution runs (3.5–7 km grid) reproduce the proper development of the clouds after 12 LT that is consistent to the observations. The total hydrometeor content and rainfall rate increase with the grid size. As a result, the rainfall amount tends to be too large compared to the observation in case of coarse resolution runs. Such systematic relationship of resolution dependency is also confirmed in the monthly averaged state. These results provide useful information on the simulation of the precipitation diurnal cycle by regional and global models that do not secure sufficient resolution for explicitly resolving the cloud systems. Additionally, a finer resolution at ≤ 7 km appears to be necessary to obtain realistic phase of the precipitation diurnal cycle over the Tibetan Plateau.

According to the theoretical consideration, initial convection that is caused by unstable stratification has the horizontal scale smaller than the coarser model (G28) resolution. Hence, it is not resolvable by the G28 run. The G3.5 run can somehow resolve the convection initially occurred by the surface heating, which consequently conducts to proper simulation of the convection start. As vertical profile becomes more unstable, the vertical convection which has larger horizontal scale can be developed. Therefore, relatively lower resolution runs are capable of resolving the convection at this moment, although its intensity may be too strong because of the larger surface fluxes. Numerical experiments further indicate that the coarser resolution run tends to overestimate the water cycle between land and atmosphere.

Acknowledgements

We acknowledge F. Kimura, W. Yanase, M. Hara, and S. Yokoi for their useful comments and discussions. Constructive comments and suggestions by two anonymous reviewers were extremely helpful to improve the manuscript. Radiative transfer code to evaluate brightness temperature was provided by H. Owada in Japan meteorological agency. One of us (T.S) was supported by Japan Society for the Promotion of Science (JSPS) as a research fellow. The GMS and GOES data were obtained by Kochi University. This study was financially supported by Grant-in Aid for Scientific Research (20840013) by MEXT and by CREST (Core Research for Evolutional Science and Technology) program of JST (Japan Science and Technology Agency).

References

Arakawa, O. and A. Kitoh, 2005: Rainfall diurnal variation over the Indonesian maritime continent simulated by 20 km-mesh GCM. *SOLA*, **1**, 109–112, doi: 10.2151/sola2005-029.

Arakawa, A. and W.H. Schubert, 1974: Interaction of a cumulus cloud ensemble with the large-scale environment, Part I. *J. Atmos. Sci*., **31**, 674–701.

Bryan, G.H., J.C. Wyngaard, and J.M. Fritsch, 2003: Resolution requirements for the simulation of deep moist convection. *Mon. Wea. Rev*., **131**, 2394–2416.

Chen, F. and J. Dudia, 2000: Coupling an advanced land-surface/hydrology model with the Penn State/NCAR MM5 modeling system. Part I: Model description and implementation. *Mon. Wea. Rev*., **129**, 569–585.

Collier, J.C., and K.P. Bowman, 2004: Diurnal cycle of tropical precipitation in a general circulation model. *J. Geophys. Res*., **109**, D17105, doi:10.1029/2004JD004818.

Dai, A., 2001: Global precipitation and thunderstorm frequencies. Part II: Diurnal variations. *J. Climate*, **14**, 1112–1128.

Dai, A., 2006: Precipitation characteristics in eighteen coupled climate models. *J. Climate*, **19**, 4605–4630.

Dai, A., X. Lin, and K.L. Hsu, 2007: The frequency, intensity, and diurnal cycle of precipitation in surface and satellite observations over low- and mid-latitudes. *Clim. Dyn*., **29**, 727–744, doi: 10.1007/s00382-007-0260-y.

Dai, A. and K.E. Trenberth, 2004: The diurnal cycle and its depiction in the Community Climate System Model. *J. Climate*, **17**, 930–951.

Dudia, J., 1989: Numerical study of convection observed during the winter monsoon experiment using a mesoscale two-dimensional model. *J. Atmos. Sci*., **46**, 3077–3107.

Fujinami, H. and T. Yasunari, 2001: The seasonal and intraseasonal variability of diurnal cloud activity over the Tibetan Plateau. *J. Meteor. Soc. Japan*, **79**, 1207–1227.

Grabowski, W.W., 2001: Coupling cloud processes with the large-scale dynamics using the Cloud-Resolving Convection Parameterization (CRCP). *J. Atmos. Sci*., **58**, 978–997.

Hahn, D.G. and S. Manabe, 1975: The role of mountains in the south Asian monsoon circulation. *J. Atmos. Sci*., **32**, 1515–1541.

Hirose, M. and K. Nakamura, 2005: Spatial and diurnal variation of precipitation systems over Asia observed by the TRMM Precipitation Radar. *J. Geophys. Res*., **110**, D05106, doi:10.1029/2004JD004815.

Inoue, T., M. Satoh, H. Miura, and B. Mapes, 2008: Characteristics of cloud size of deep convection simulated by a global cloud resolving model. *J. Meteor. Soc. Japan*, **86A**, 17–31.

Janjic, Z.I., 2002: Nonsingular implementation of the Mellor-Yamada level 2.5 scheme in the NCEP meso model. *NCEP Office Note*, **437**, 61 pp.

Khairoutdinov, M.F. and D.A. Randall, 2001: A cloud resolving model as a cloud parameterization in the NCAR community climate system model: Preliminary results. *Geophys. Res. Lett*., **28**(18), 3617–3620.

Kuo, H.L., 1974: Further studies of the parameterization of the influence of cumulus convection on large-scale flow. *J. Atmos. Sci*., **31**, 1232–1240.

Kurosaki, Y. and F. Kimura, 2002: Relationship between topography and daytime cloud activity around Tibetan Plateau. *J. Meteor. Soc. Japan*, **80**, 1339–1355.

Kuwagata, T., A. Numaguti, and N. Endo, 2001: Diurnal variation of water vapor over the central Tibetan Plateau during summer. *J. Meteor. Soc. Japan*, **79**, 401–418.

Liu, Y., B. Hoskins, and M. Blackburn, 2007: Impact of Tibetan orography and heating on the summer flow over Asia. *J. Meteor. Soc. Japan*, **85**, 2B, 1–19.

Miura, H., H. Tomita, T. Nasuno, S. Iga, M. Satoh, and T. Matsuno, 2005: A climate sensitivity test using a global cloud resolving model under an aqua planet condition. *Geophys. Res. Lett*., **32**, L19717, doi:10.1029/2005GL023672.

Miura, H., M. Satoh, H. Tomita, T. Nasuno, S. Iga, and A.T. Noda, 2007a: A short-duration global cloud-resolving simulation with a realistic land and sea distribution. *Geophys. Res. Lett*., **34**, L02804, doi:10.1029/2006GL027448.

Miura, H., M. Satoh, T. Nasuno, A.T. Noda, and K. Oouchi, 2007b: An Madden-Julian Oscillation event simulated using a global cloud-resolving model. *Science*, **318**, 1763–1765.

Mlawer, E.J., S.J. Taubman, P.D. Brown, M.J. Iacono, and S.A. Clough, 1997: Radiative trans-fer for inhomogeneous atmosphere: RRTM, a validated correlated-k model for the long-wave. *J. Geophys. Res*., **102**(D14), 16663–16682.

Molinari, J. and M. Dudek, 1992: Parameterization of convective precipitation in mesoscale numerical models: A critical review. *Mon. Wea. Rev*., **120**, 326–344.

Murata, A., K. Saito, and M. Ueno, 2003: The effects of precipitation schemes and horizontal resolution on the major rainband in typhoon Flo (1990) predicted by the MRI mesoscale nonhydrostatic model. *Meteor. Atmos. Phys*., **82**, 55–73.

Nagasawa, R., T. Iwasaki, S. Asano, K. Saito, and H. Okamoto, 2006: Resolution dependence of non-hydrostatic models in simulating the forma-

tion and evolution of low-level clouds during a "Yamase" event. *J. Meteor. Soc. Japan*, **84**, 969–987.

Neale, R. and J. Slingo, 2003: The maritime continent and its role in the global climate: A GCM study. *J. Climate*, **16**, 834–848.

Owada, H., 2006: Satellite imagery from numerical weather prediction models. *Meteor. Res. Note*, **212**, 105–120 (in Japanese).

Petch, J.C., A.R. Brown, and M.E.B. Gray, 2002: The impact of horizontal resolution on the simulations of convective development over land. *Quart. J. Roy. Meteor. Soc.*, **128**, 2031–2044.

Sato, T. and F. Kimura, 2005: Impact of diabatic heating over the Tibetan plateau on subsidence over Northeast Asian arid region. *Geophys. Res. Lett.*, **32**, L05809, doi:10.1029/2004GL022089.

Sato, T. and F. Kimura, 2007: How does the Tibetan Plateau affect the transition of Indian monsoon rainfall? *Mon. Wea. Rev.*, **135**, 2006–2015.

Sato, T., H. Miura, and M. Satoh, 2007: Spring diurnal cycle of clouds over Tibetan Plateau: global cloud-resolving simulations and satellite observations. *Geophys. Res. Lett.*, **34**, L18816, doi:10.1029/2007GL030782.

Satoh, M., T. Matsuno, H. Tomita, H. Miura, T. Nasuno, and S. Iga, 2008: Nonhydrostatic Icosahedral Atmospheric Model (NICAM) for global cloud resolving simulations. *J. Comput. Phys.*, **227**, 3486–3514, doi:10.1016/j.jcp.2007.02.006.

Shinoda, T. and H. Uyeda, 2002: Effective factors in the development of deep convective clouds over the wet region of eastern China during the summer monsoon season. *J. Meteor. Soc. Japan*, **80**, 1395–1414.

Skamarock, W.C., J.B. Klemp, J. Dudhia, D.O. Gill, D.M. Barker, W. Wang, and J.G. Powers, 2005: A description of the advanced research WRF version 2, *NCAR/TN-468+STR*, 88 pp.

Slingo, A., K.I. Hodges, and G.J. Robinson, 2004: Simulation of the diurnal cycle in a climate model and its evaluation using data from Meteosat 7. *Quart. J. Roy. Meteor. Soc.*, **130**, 1449–1467.

Stevens, D.E., A.S. Ackerman, and C.S. Bretherton, 2002: Effects of domain size and numerical resolution on the simulation of shallow cumulus convection. *J. Atmos. Sci.*, **59**, 3285–3301.

Tomita, H. and M. Satoh, 2004: A new dynamical framework of nonhydrostatic global model using the icosahedral grid. *Fluid Dyn. Res.*, **34**, 357–400.

Tomita, H., H. Miura, S. Iga, T. Nasuno, and M. Satoh, 2005: A global cloud-resolving simulation: preliminary results from an aqua planet experiment. *Geophys. Res. Lett.*, **32**, L08805, doi:10.1029/2005GL022459.

Weisman, M.L., W.C. Skamarock, and J.B. Klemp, 1997: The resolution dependence of explicitly modeled convective systems. *Mon. Wea. Rev.*, **125**, 527–548.

Wu, G.X. and Y.S. Zhang, 1998: Tibetan plateau forcing and the timing of the monsoon onset over South Asia and the South China Sea. *Mon. Wea. Rev.*, **126**, 913–927.